Bridging the Gap: A Unified Mathematical Model for Standardising Glenoid Bone Loss Measurement

Alexander Gallant [1]*, Quinten Mortier [2], Anne Karelse [2 3], Alexander Van Tongel [2 3]

(*) Corresponding author: alexandergallant@posteo.net
1. Jan Yperman Hospital, Briekestraat 12, 8900 Ieper, Belgium
2. UGent, Sint-Pietersnieuwstraat 33, 9000 Gent, Belgium
3. UZ Gent, Corneel Heymanslaan 10, 9000 Gent, Belgium

Background: A major factor in recurrent traumatic anterior shoulder instability is glenoid bone loss, often caused by bony Bankart lesions. Accurate quantification of glenoid bone loss is essential for determining appropriate treatment. Numerous measurement indexes have been proposed, but variability in methodologies complicates comparisons across studies and clinical decision-making.

Purpose: To develop a conversion table to allow comparison between different indexes.

Methods: This study identified 11 commonly used glenoid bone loss indexes from the literature. These indexes measure bone loss using different parameters, including linear measurements, surface area calculations, and ratios derived from 2D CT images or 3D reconstructions. A conversion table was developed to establish correlations between these indexes using Sugaya's method as the reference.

Results: Mathematical relationships between bone loss expressed as a percentage of glenoid width, surface area, and chord length were derived using basic formulas for circular segments. This demonstrated that linear measurement-based indexes tend to overestimate bone loss compared to surface area-based methods. A conversion table was created to facilitate direct comparisons between the different indexes.

Conclusion: The proposed conversion table enables the conversion of glenoid bone loss values between different measurement methods. This tool enhances data conversion across studies, improves the accuracy of bone loss evaluation, and aids in clinical decision-making. Converting measurements will reduce discrepancies between linear and surface area-based methods, ultimately benefiting surgical planning and treatment selection.

What this study adds: The authors feel this study adds the tools to allow both better understanding of the different aspects of glenoid bone loss and conversion of values between existing indexes.

Potential impacts on research, practice or policy: The results of this study enhance data conversion across studies, improves the accuracy of bone loss evaluation, and aids in clinical decision-making.

Study Design: Retrospective imaging and mathematical modelling study using 3D CT reconstructions

Level of Evidence: IV

Keywords: Glenoid Bone Loss, Shoulder Instability, Latarjet, Index, Quantification, Conversion Table

https://doi.org/10.70885/hmsj.2026.02.003

Introduction

The optimal surgical management of recurrent anterior shoulder instability remains a subject of ongoing debate [1][2][3][4][5][6][7][8][9][10][11][12][13][14][15]. While bony reconstruction procedures have demonstrated reliable stability, especially in the presence of significant glenoid bone loss, concerns regarding complication rates, altered anatomy, and long-term outcomes persist [16][17][18][19][20][21][22][23][24][25]. This has led many authors to advocate for a more individualised treatment strategy balancing patient-specific factors - such as age, activity level, and recurrence risk - with disease-specific parameters, most notably the extent of glenoid bone loss [2][12][26][27][28]. It has been shown that the extent of glenoid bone loss alone does not provide an adequate estimation of the actual biomechanical effect of glenoid defects, suggesting it might be unwise to tailor treatment based solely on this parameter [12].

Within this context, however, the quantification of glenoid bone loss still has become one of the determinants aiding in selecting between soft tissue stabilisation and bony augmentation procedures [1][3][4][5][9][10][29][30][31][32][33]

[34][35]. Numerous biomechanical and clinical studies have proposed threshold values of bone loss beyond which isolated soft tissue repair may be insufficient. However, reported cut-off values vary widely across the literature, with recommendations for bony reconstruction ranging from as low as 13.5% to more than 25% glenoid bone loss [14][36][37][38][39][40][41][42].

Indeed, multiple measurement indexes have been introduced, each based on different geometric assumptions and imaging techniques [6][7][8][33][34][35][43][44][45][46][47][48]. Some methods rely on linear width measurements of the glenoid, whereas others estimate surface area loss or incorporate three-dimensional curvature of the glenoid socket. As a consequence, identical anatomical defects may be reported as substantially different degrees of bone loss depending on the chosen index.

Weil et al. have addressed fact that the significant heterogenicity in both the imaging modality and method used to measure glenoid bone loss have made it very difficult to determine whether any published paper should influence clinical practice or should be dismissed [13]. Furthermore, Bakshi et al. and Chalmers et al. have shown in basic terms that width-based methods tend to assess the glenoid defect as a larger percentage compared to surface area-based methods [49][50]. Despite this, the magnitude of their impact on reported bone loss values has not been systematically explored.

The aim of this study is to identify measurement indexes for glenoid bone loss in literature and - since these are mostly mathematically linked - develop a geometry-based conversion framework (with tabulated values) mapping linear, chord, and area measurements to each other under the circular-segment assumption. This table will enable direct conversions between different methods of quantifying glenoid bone loss.

Materials and Methods

Indexes

Eleven indexes were identified in literature. An overview with their specific traits is given in **Table 1**. Measurements were done on 2D CT images or on 3D reconstructions based on CT images. The measurements themselves could be linear measurements between two or more points, or area methods. Noteworthy, some of the linear measurements calculate a surface area based on these linear measurements. Therefore, some indexes measure the bone loss as a part of the diameter, glenoid height or the chord of the defect whilst other measure the bone loss as a part of the surface area of the inferior glenoid circle. A visual representation of these concepts is given in **Figure 1**.

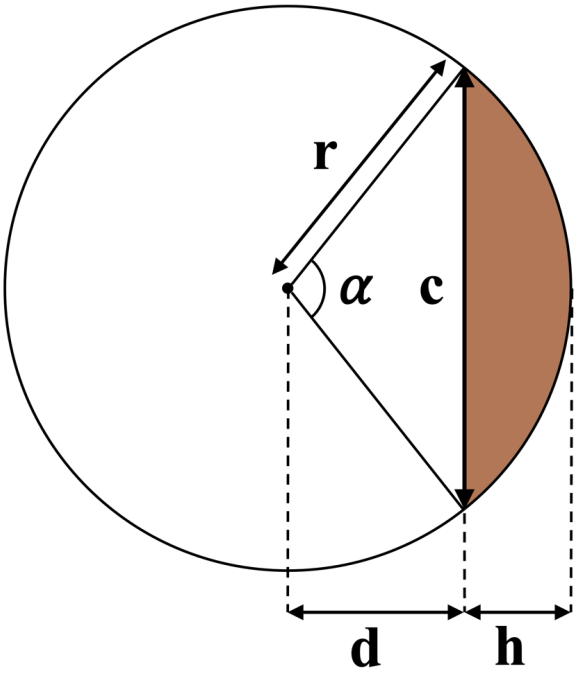


Figure 1. Schematic representation of the defect in the inferior glenoid circle. This corresponds to a lateral view of the glenoid and the inferior glenoid circle. Definitions for the parameters used here and throughout the article: r = radius of the circle, h = sagitta (height) of the circular segment, d = r − h, c = chord of the circular segment, α = central angle (in radians), A = area of circular segment (orange/darker zone)

Index	2D/3D	Measurement
Sugaya method	3D	Fits inferior glenoid circle on injured shoulder and determines bone loss as the sagitta divided by the diameter of the circle and expressed as a percentage.
Griffith index (W)	2D	Their most reliable measurement was simply comparing the glenoid width (measured perpendicular to the vertical axis) of the injured side to that of the uninjured side.
Griffith index (L)	2D	Ratio of the width of the glenoid (i.e. the diameter of the circle minus the sagitta) to the length of the glenoid, predisposes for instability when this ratio is smaller than 0.7.
Gerber index	2D	Ratio of the chord length (= the length of the defect itself) over the diameter of the circle minus the sagitta of the defect.
Glenoid index	3D	Ratio of the diameter of the inferior glenoid circle minus the sagitta of the defect to the diameter of the inferior glenoid circle, calculated by drawing the inferior glenoid circle on the unaffected shoulder, dividing this by the glenoid length of the uninjured shoulder and multiplying this by the glenoid length of the injured shoulder.
PICO method	2D	Ratio of the surface area of the bony fragment and the surface area of the inferior glenoid circle of injured side. When the bony fragment is not present, use the inferior glenoid circle of the uninjured site as a reference to calculate the same index. Expressed as a percentage.
Sugaya's area method	3D	Calculates the same ratio as PICO method but on a 3D image and only based on the inferior glenoid circle of the injured side.
Barchilon's method	2D or 3D	Inferior glenoid circle marked and radius (r) and radius minus sagitta (d) measured in this image. Surface area of defect compared to the total surface area of the inferior glenoid circle was calculated and expressed as a percentage as follows: $\frac{1}{\pi}\left(cos^{-1}\left(\frac{d}{r}\right)-\left(\frac{d}{r}\sqrt{1-\left(\frac{d}{r}\right)^2}\right)\right)\times 100$
Dumont's method	3D	Measure the opening angle (α) of the defect and calculating the bone loss expressed as a percentage as follows: $\frac{\alpha - sin\left(\alpha\right)}{2\pi}\times 100$
Parada's method	3D	Calculate the opening angle (α) of the defect from the chord length (c) as follows: $=2arcsin\frac{c}{2r}$ Then calculate the bone loss expressed as a percentage via the formula used in Dumont's method.
McNeil's method	3D	Measures the attrition of the bony fragment by calculating the ratio of the surface area of the leftover fragment to the surface area of the defect.
De Filippo's method	3D	Measures the defect size of the glenoid surface compared to the total glenoid surface on a curved surface.

This table lists if measurements were done in 2D or 3D views and how each index was measured. Eleven indexes were identified in literature. An overview with their specific traits is given.

Mathematical correlation and conversion

The first aim of the study was to make a general conversion between the bone loss as a percentage of the diameter and the bone loss as a percentage of the surface area of the inferior glenoid circle. Furthermore, a general conversion between the above mentioned values and the bone loss in function of the chord of the defect was calculated. In order to calculate these values, some basic mathematical formulas that apply to a circular segment were necessary, these are added in the **Appendix**.

These basic formulas were then used to calculate the mathematical link between all indexes provided in **Table 1**. Note in this case that it is impossible to calculate the percentage of width defect from an area value (e.g. it is impossible to calculate the glenoid index from the PICO method). It has been analytically proven that there is no closed-form expression for h as a function of A given the 'arcsin(x) – x' component in the formula. For this reason, an index based on a width measurement was chosen as the reference value to calculate all other indexes (including the surface area indexes). An index based on a measurement on

a 3D reconstruction and a simple index referencing the percentage width loss was preferred. For this reason, Sugaya's linear method was chosen as the reference value – being solely a mathematical consideration [8].

De Filippo's method was an exception that could not be calculated directly. De Filippo's method can in a simplified form be considered as a partial loss of the surface area of a spherical cap, elucidated in the results section and illustrated in **Figure 2**. To calculate the integral necessary to model this surface area, the value of θ, the polar angle of the spherical cap, has to be known.

To quantify this angle, we retrospectively analysed 3D CT images. After obtaining approval from the Ethical Committee of Ghent University Hospital, patients were identified and recruited from an existing database of patients receiving a bilateral CT (e.g. due to protocol for polytrauma patients) in the same institution. The non-affected, intact shoulders in these scans were retained for analysis. A total of 143 intact scapulae were retained for further analysis.

These were analysed using Mimics (Materialise, 21.0) to calculate a three-dimensional reconstruction of the scapula, mark the most anterior, posterior and inferior point on the glenoid rim, calculate the inferior glenoid circle and construct the best fitting sphere in the glenoid socket based on the surface contact with the area covered by the inferior glenoid circle [51][52][53]. The values of these points and spheres were then imported into MATLAB software (MathWorks, R2021a) to calculate the polar angle θ of the spherical cap. Maple software (Maple 2024.1) was used to solve the integral for the spherical cap defect. The online Desmos software was used to generate graphs.

Results

Correlation between the linear defect and the surface area defect

To calculate the curve for the correlation between the sagitta h (or linear defect) and the area A (or surface area of the defect), we take the fourth formula (for A, the surface area of the defect) shown in the appendix divided by πr^2 (relative surface of the area of the defect compared to the total surface area of the circle). We multiply by 100 to consider the diameter as 100% (=100), so r becomes 50. Using the first formula from the appendix, substitute c to obtain the relation to the sagitta h. This gives us the following formula for the curve:

$$A = \frac{\left(100\left(\arcsin\sqrt{\frac{2h}{50}-\frac{h^2}{2500}}-\left(1-\frac{h}{50}\right)\sqrt{\frac{2h}{50}-\frac{h^2}{2500}}\right)\right)}{\pi} for 0 \le h \le 50\,(\%)$$

Figure 3 shows a visual representation of this curve up to 50% bone loss on the glenoid (sagitta h plotted on the x-axis, area A plotted on the y-axis). This indicates, as previously shown, that indexes based on the width of the glenoid tend to overestimate the bone loss compared to area methods in defects smaller than 50%, and the overestimation is generally larger for smaller defects.

To calculate the curve for the correlation between the chord c and the sagitta h, we take the first formula (for c) from the appendix and substitute r for the value of 50 to acquire this as a percentage as demonstrated above. Rewriting this formula to express h in function of c shows:

$$h = 50 - \sqrt{2500 - \frac{c^2}{4}} for 0 \le h \le 50\,(\%)$$

To calculate the curve for the correlation between the chord c and the area A, we take the fourth formula (for A) from the appendix and substitute the value of 50 for r to acquire this as a percentage as demonstrated above.

$$A = \frac{100\left(\arcsin\frac{c}{100}-\frac{c}{100}\sqrt{1-\left(\frac{c}{100}\right)^2}\right)}{\pi} for 0 \le A \le 50\,(\%)$$

Figure 4 shows a visual representation of the sagitta h and the area A (both plotted on the y-axis) compared to the chord of the defect (plotted on the x-axis) up to 50% bone loss.

Calculation of the correlations between the different indexes

To calculate the correlations between all indexes referred in **Table 1**, we correlated each index to our reference index. Sugaya's method was chosen as the reference index for reasons listed above. Below is the description of the calculation of the correlation of all indexes to our reference index.

Sugaya Method

The reference index. Let Sugaya's Index = f(S). This index is equal to the ratio of the sagitta h to the diameter of the inferior glenoid circle (= two times the radius) [8]. Rewriting this to express the sagitta h in function of this index we get:

$$f(S) = \frac{h}{2r}\{1\}$$
$$\iff h = 2rf(S)\{2\}$$

The calculations of all formulas for the different indexes are added as supplementary information at the end of this article.

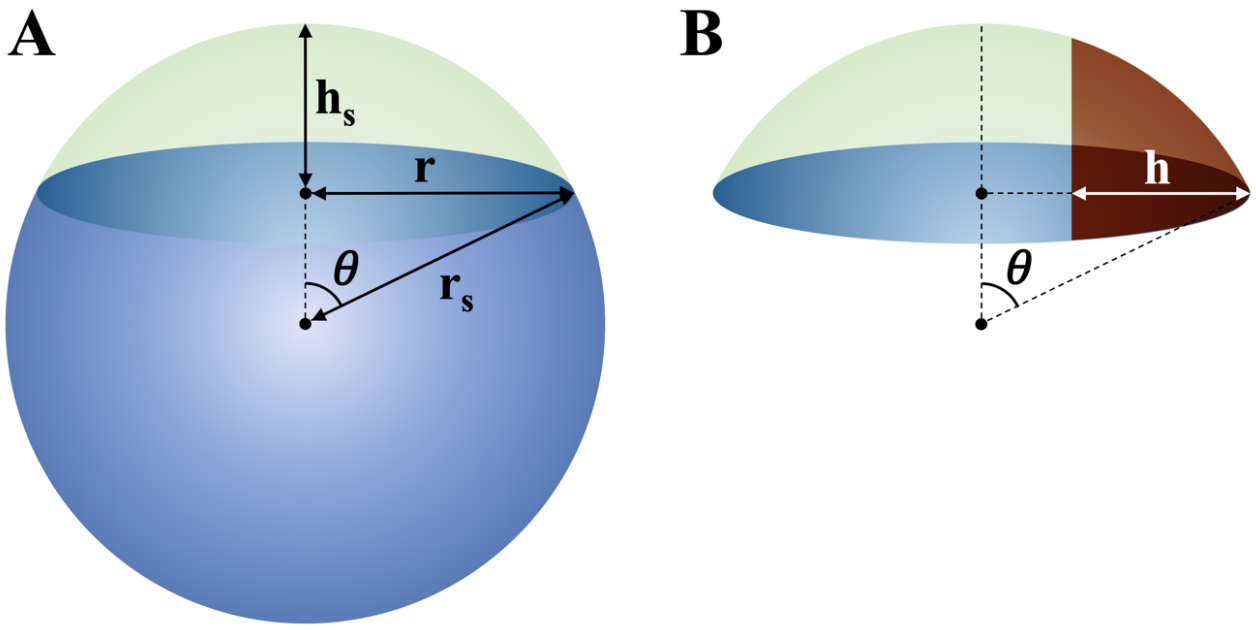


Figure 2: Schematic representation of a spherical cap. (A) shows the spherical cap in green/lighter colour resting on top of the rest of the sphere in blue/darker colour. The spherical cap can be considered the contact surface of the curved glenoid. (B) shows an isolated spherical cap in green/lighter colour with the defect of the glenoid surface marked in brown/dark. Definitions for the parameters used here and throughout the article: r_s = radius of the sphere, h_s = sagitta (height) of the spherical cap, r = radius of the base circle of the spherical cap = the inferior glenoid circle, D = the diameter of the inferior glenoid circle = $2r$, h = the sagitta of the defect on the inferior glenoid circle, θ = polar angle (angle between the rays from the centre of the sphere to the apex of the cap (pole) and the edge of the circle forming the base of the cap), A_s = surface area of spherical cap (green/lighter zone in A), A_d = surface area of the defect (brown/dark zone in B).

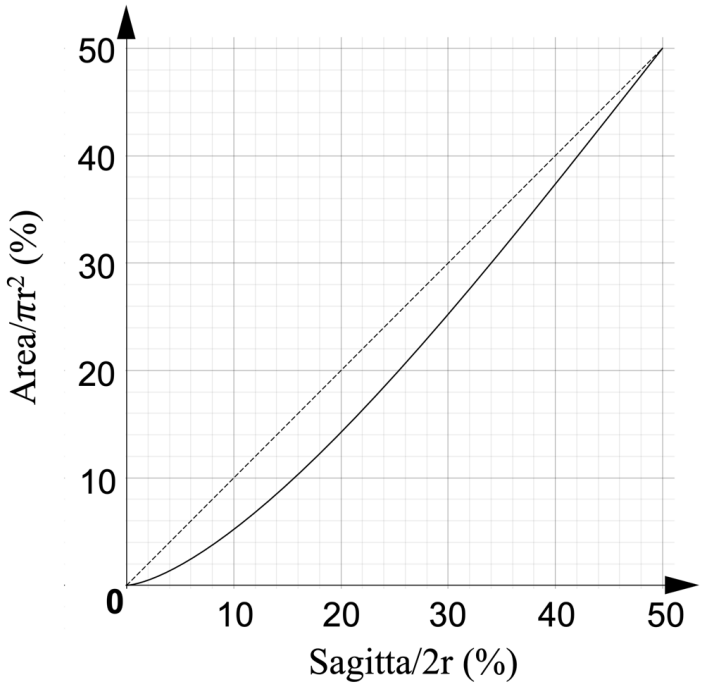


Figure 3: Graphic representation of the correlation between the sagitta h as a percentage of $2r$ plotted on the x-axis in % and the area A as a percentage of the total surface area of the inferior glenoid circle (=πr^2) plotted on the y-axis in % up to 50% bone loss on the glenoid. The dashed line marks the bisector of the first quadrant.

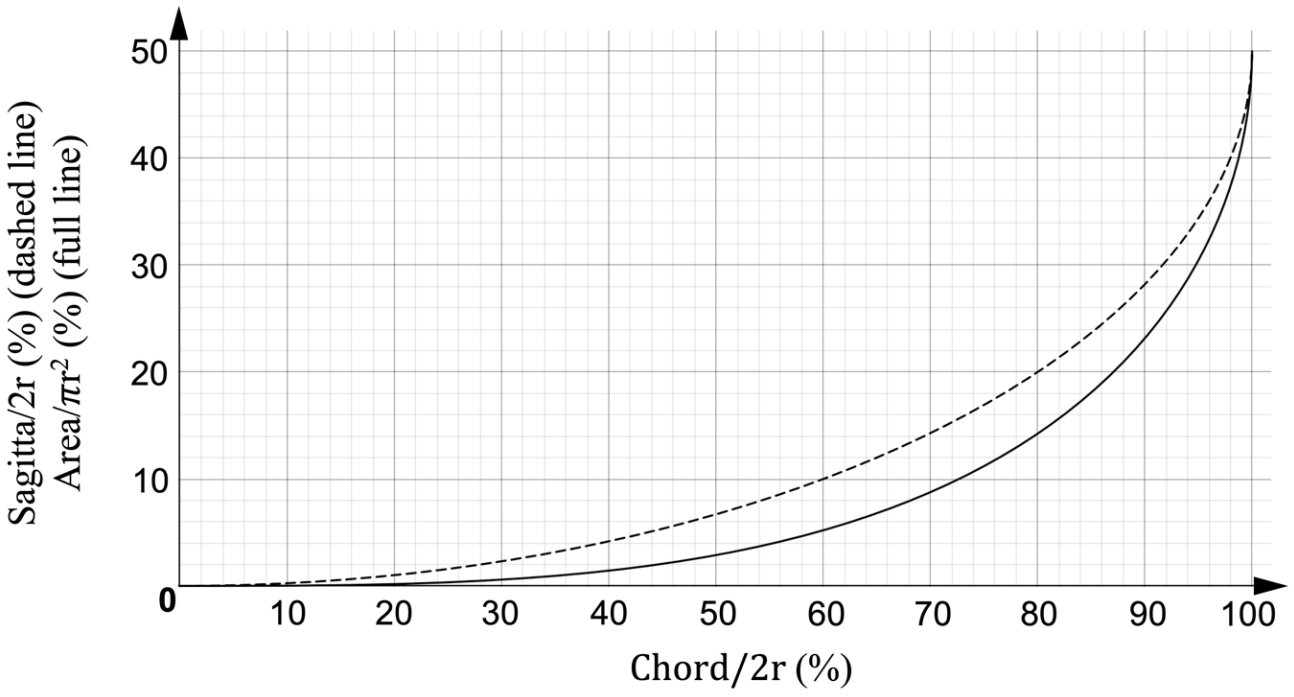


Figure 4: Graphic representation of the correlation between the chord c as a percentage of $2r$ plotted on the x-axis in % and the sagitta h as a percentage of $2r$ and area A as a percentage of the total surface area of the inferior glenoid circle (=πr^2) both plotted on the y-axis in % up to 50% bone loss on the glenoid. The dashed line represents the correlation of the chord to the sagitta, the full line represents the correlation of the chord to the area.

Grittith Index

The original paper of Grittith et al. proposed various measurements and reported that the most reliable measurement is simply comparing the glenoid width (measured perpendicular to the vertical axis) of the injured side to that of the uninjured side (Griffith Index (W)) [44]. Chuang et al. modified this in 2008 by adding the width of the inferior glenoid circle on the injured side as a reference for the width of the uninjured glenoid [34]. For this analysis, since there is no info on the uninjured side calculable from an index, we adopted the diameter of the inferior glenoid circle on the injured side as reference for the native glenoid width. This makes this method essentially the same as Sugaya's method described above. Griffith et al. also suggest the ratio of the width of the glenoid (i.e. the diameter of the circle minus the sagitta) to the length of the glenoid predisposes for instability when this ratio is smaller than 0.7 (Griffith Index (L)) [44]. Recently, Makovicka et al. showed that 2/3 of the glenoid height is a reliable parameter to map the inferior glenoid circle [32]. Thus 2/3 of the glenoid height approximates the diameter of the inferior glenoid circle, indicating that the glenoid height is approximately equal to thrice the radius of the inferior circle.

Gerber Index

The Gerber Index calculates the ratio of the chord length (= the length of the defect itself) over the diameter of the circle minus the sagitta of the defect [43].

Glenoid Index

The Glenoid Index expresses the ratio of the diameter of the inferior glenoid circle minus the sagitta of the defect to the diameter of the inferior glenoid circle, calculated by drawing the inferior glenoid circle on the unaffected shoulder, dividing this by the glenoid length of the uninjured shoulder and multiplying this by the glenoid length of the injured shoulder [34]. There is some recent evidence indicating that the inferior glenoid circle drawn on a glenoid with a defect might not accurately represent the original width of the glenoid. Due to the posteroinferior geometry, measurements tend to overestimate the diameter (and thus the relative defect size) [10][11]. Since the glenoid length and width of the uninjured shoulder can impossibly be calculated from the glenoid index, this study did calculate the glenoid width of the injured side based on the width of the inferior glenoid circle of the injured side.

Area methods

Note that all area methods (PICO method, Sugaya's adaptation of PICO method, Barchilon's method, Dumont's

method and Parada's method) except for McNeil's method accounting for the attrition of the bony fragment measure essentially the same value by different means, namely the surface area of the bone loss compared to the total surface area of the inferior glenoid circle [6][35][46][47][48]. In our study, we consider the mathematical link between these indexes and disregard measurement variances since these are theoretically the same. The value for these indexes is thus equal. We can express this value as the formula for the surface area of the defect calculated in the first section where we calculate the surface area of the defect in function of the sagitta and divide this by the surface area of the inferior glenoid circle (the radius of the circle squared times pi).

McNeil's method

McNeil's method measured the attrition of the bony fragment by comparing the leftover size of the bony fragment to the surface defect in the inferior glenoid circle [7]. More attrition of the bony fragment (i.e. a larger discrepancy between the leftover bony fragment and the defect size) leads to a higher percentage attritional bone loss. This value was impossible to calculate and could not be added in the conversion table.

Literature does show some reinterpretation of this index or the above indexes and reported the use of the ratio of the surface area of the defect to the total surface area of the inferior circle minus the surface area of the defect [33].

De Filippo's method

De Filippo's method measures bone loss on a curved three-dimensional glenoid surface rather than a flat representation of this surface [45]. Whilst this is impossible to simulate in a mathematical formula due to the variable pear-shape of the glenoid, this study adapted an approach similar to the technique reported in the PICO method or other similar indexes described above, i.e. it calculates the percentage bone loss compared to the inferior glenoid circle but mapping this on a curved surface area. The authors acknowledge that this is not an exact translation of this index in the conversion table, but does offer some insights into the variation in defect assessment when considering a flat or curved inferior glenoid circle. As previously referenced, **Figure 2** illustrates a spherical cap and the definitions used. The spherical cap is represented by the green/lighter zone in **Figure 2A**. The basic formulas to calculate the surface area of a spherical cap are given in the appendix section.

The aim is to calculate the leftover surface area of the spherical cap after bone loss has occurred. To account for varying degrees of bone loss, intersect the spherical cap with a plane perpendicular to the plane that separates the spherical cap from the rest of the sphere. This plane will split the cap into two pieces: one will be the leftover glenoid (the green/lighter zone in **Figure 2B**), the other is the amount of bone lost (the brown/dark zone in **Figure 2B**). Note that the base circle of this cap equals the inferior glenoid circle, thus the sagitta h and the radius r illustrated in **Figure 2** are still the same sagitta and radius referenced in **Figure 1** for all other methods. The new sagitta of the spherical cap itself is represented by h_s and the radius of the sphere itself is represented by r_s. To define the percentage of glenoid surface area lost (or percentage of surface area leftover) in function of the length of the sagitta h, the following integral was solved:

$$A_s = \int_{r-h}^{r} dy \int_{-\sqrt{r^2-y^2}}^{\sqrt{r^2-y^2}} dx \frac{r_s}{\sqrt{r_s^2 - x^2 - y^2}}$$

Since this must be defined as a percentage loss (i.e. the surface area of the bone deficit (A_d) has to be expressed as a percentage of the total surface area of the spherical cap (A_s)) in function of the length of h as a percentage of the diameter of the inferior glenoid circle (D), this can be calculated and rewritten as follows:

$$A_d = \frac{\pi(1-\cos(\theta)) - 2\cos(\theta)\arcsin\left(\frac{h}{50}-1\right) 100\Big(-2\left(1-\frac{h}{50}\right)\sin(\theta)\arctan\left(\tan(\theta)\sqrt{\frac{h}{50}\left(2-\frac{h}{50}\right)}\right) - \arctan\left(\frac{\sin(\theta)-\frac{h}{50}+1}{\cos(\theta)\sqrt{\frac{h}{50}\left(2-\frac{h}{50}\right)}}\right) + \arctan\left(\frac{\sin(\theta)+\frac{h}{50}-1}{\cos(\theta)\sqrt{\frac{h}{50}\left(2-\frac{h}{50}\right)}}\right)\Big)}{2\pi(1-\cos(\theta))}$$

As mentioned before, this formula could not be straightforwardly calculated into exact values without knowing the average value of the polar angle θ. We measured θ on 143 scapulae showing an average value of 13,22 degrees (0,231 radians) with a standard deviation (SD) of 6,90 degrees (0.120 radians). The values for De Filippo's method were calculated using the 0.231 radians value (close to a flat circle). This showed values never exceeding 0.10% difference to the PICO method. The same values were subsequently calculated using 0.351 (the average value + the standard deviation), showing values never exceeding 0.22% difference to the PICO method. Using this θ-value assumes generalizability of the data used in this study. It is noteworthy, however, that differences between flat and curved area measurements remained near-infinitesimally small when using the +1SD value for θ (i.e. a strongly curved glenoid in our dataset).

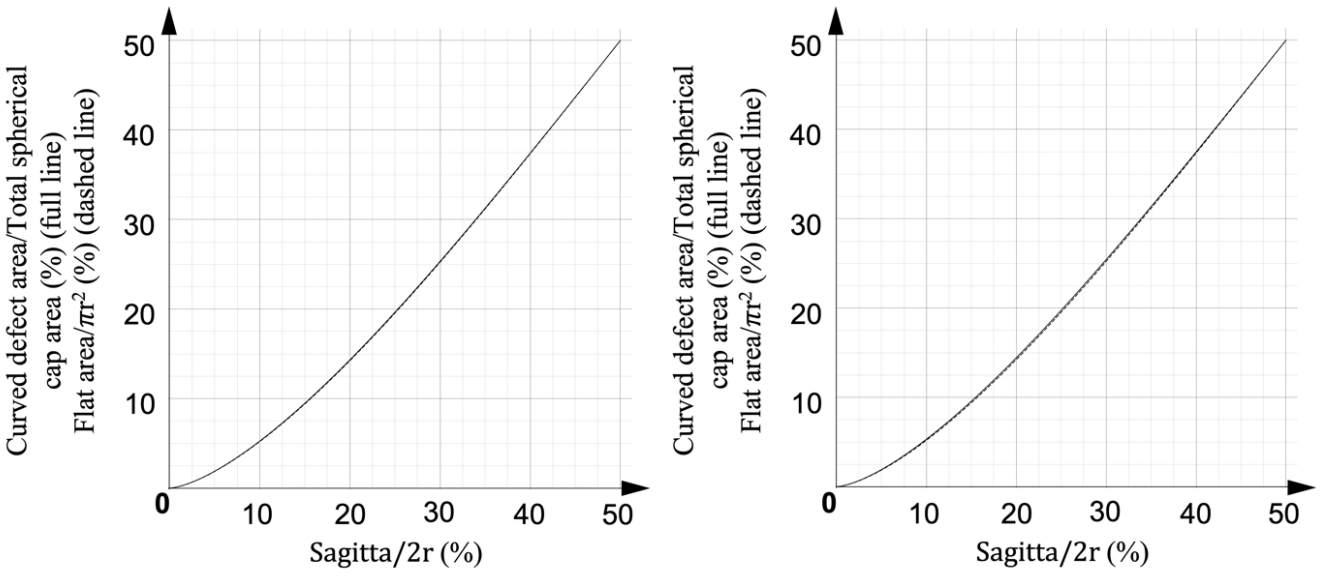


Figure 5. Graphic representation of the correlation of the surface area of the defect on a flat inferior glenoid circle as a percentage of the total surface area of the inferior glenoid circle (=πr^2) (y-axis) to the sagitta h as a percentage of $2r$ (x-axis) compared to the correlation of the surface area of the defect on a curved inferior glenoid spherical cap as a percentage of the total surface area of the spherical cap (y-axis) to the sagitta h as a percentage of $2r$ (x-axis). The flat surface area curve is represented as a dashed line, the curved surface area curve is represented as a full line. Figure 5.1 (left) shows these curves with a polar angle of 0.231, figure 5.2 (right) shows these curves with a polar angle of 0.351.

Figure 5 shows the curve of the correlation of the surface area of the defect on a flat inferior glenoid circle as a percentage of the total surface area of the inferior glenoid circle (=πr^2) (y-axis) to the sagitta h as a percentage of $2r$ (x-axis) compared to the correlation of the surface area of the defect on a curved inferior glenoid spherical cap as a percentage of the total surface area of the spherical cap (y-axis) to the sagitta h as a percentage of $2r$ (x-axis). The flat surface area curve is represented as a dashed line, the curved surface area curve is represented as a full line. **Figure 5.1** shows these curves with a polar angle of 0.231, **Figure 5.2** shows these curves with a polar angle of 0.351. Note that these two curves are nearly indistinguishable, even in **Figure 5.2**.

Final table

Table 2 shows the values of the reference index, Sugaya's Index, in increments of 1 percent up to 50% and shows the relative values of all other indexes included in this article to allow for easy conversion of values between indexes. De Filippo's method was calculated using 0.231 as the value for θ.

Discussion

Quantification of glenoid bone loss can be an influential factor for assessment of shoulder instability and determining appropriate treatment strategies. However, the significant heterogenicity in both the imaging modality and method used to measure glenoid bone loss have made it very difficult to assess the impact of solitary papers and compare them to the literature [13]. This study aimed to address this challenge by developing a conversion table that establishes correlations between different bone loss indexes, thereby facilitating conversion in clinical and research settings.

One of the key insights of this study is that linear measurement-based indexes tend to overestimate glenoid bone loss compared to surface area-based methods, as had been previously suggested by Bakshi et al. and Chalmers et al.[49][50] This discrepancy arises from the geometric properties of the glenoid, where width-based calculations fail to account for the non-rectangular nature of bone loss. De Filippo's method, which accounts for spherical curvature rather than assuming a flat glenoid surface, showed very little variation compared to the flat measurement on the inferior glenoid circle (ranging up to a maximum of 0.21% difference). Even when taking the variations in polar angle into account, the value difference never exceeded 0.22%. Taking the margin for error on measurements into account, this suggests that, though this curved surface shows the most accurate representation of the in vivo situation, measurements on the inferior circle yield near identical results for a much smaller effort.

Table 2.

Sugaya Linear Method (%)	Griffith Index (ratio)	Gerber Index (ratio)	Glenoid Index (ratio)	Surface Area Methods (%)	Curved Surface Area (%)
0.00	0.67	0.00	1.00	0.00	0.00
1.00	0.66	0.20	0.99	0.17	0.17
2.00	0.65	0.29	0.98	0.48	0.48
3.00	0.65	0.35	0.97	0.87	0.88
4.00	0.64	0.41	0.96	1.34	1.36
5.00	0.63	0.46	0.95	1.87	1.89
6.00	0.63	0.51	0.94	2.45	2.48
7.00	0.62	0.55	0.93	3.08	3.11
8.00	0.61	0.59	0.92	3.75	3.79
9.00	0.61	0.63	0.91	4.46	4.50
10.00	0.60	0.67	0.90	5.20	5.25
11.00	0.59	0.70	0.89	5.98	6.04
12.00	0.59	0.74	0.88	6.80	6.86
13.00	0.58	0.77	0.87	7.64	7.70
14.00	0.57	0.81	0.86	8.51	8.58
15.00	0.57	0.84	0.85	9.41	9.48
16.00	0.56	0.87	0.84	10.33	10.40
17.00	0.55	0.91	0.83	11.27	11.35
18.00	0.55	0.94	0.82	12.24	12.32
19.00	0.54	0.97	0.81	13.23	13.31
20.00	0.53	1.00	0.80	14.24	14.33
21.00	0.53	1.03	0.79	15.27	15.36
22.00	0.52	1.06	0.78	16.31	16.40
23.00	0.51	1.09	0.77	17.38	17.47
24.00	0.51	1.12	0.76	18.45	18.55
25.00	0.50	1.15	0.75	19.55	19.64
26.00	0.49	1.19	0.74	20.66	20.75
27.00	0.49	1.22	0.73	21.78	21.88
28.00	0.48	1.25	0.72	22.92	23.01
29.00	0.47	1.28	0.71	24.07	24.16
30.00	0.47	1.31	0.70	25.23	25.32
31.00	0.46	1.34	0.69	26.40	26.49
32.00	0.45	1.37	0.68	27.59	27.67
33.00	0.45	1.40	0.67	28.78	28.86
34.00	0.44	1.44	0.66	29.98	30.06

35.00	0.43	1.47	0.65	31.19	31.26
36.00	0.43	1.50	0.64	32.41	32.48
37.00	0.42	1.53	0.63	33.64	33.70
38.00	0.41	1.57	0.62	34.87	34.93
39.00	0.41	1.60	0.61	36.11	36.17
40.00	0.40	1.63	0.60	37.35	37.41
41.00	0.39	1.67	0.59	38.60	38.65
42.00	0.39	1.70	0.58	39.86	39.90
43.00	0.38	1.74	0.57	41.12	41.16
44.00	0.37	1.77	0.56	42.38	42.41
45.00	0.37	1.81	0.55	43.64	43.67
46.00	0.36	1.85	0.54	44.91	44.93
47.00	0.35	1.88	0.53	46.18	46.20
48.00	0.35	1.92	0.52	47.45	47.47
49.00	0.34	1.96	0.51	48.73	48.73
50.00	0.33	2.00	0.50	50.00	50.00

The values of the reference index, Sugaya's Index, in increments of 1 percent up to 50% and shows the relative values of all other indexes included in this article to allow for easy conversion of values between indexes. De Filippo's method was calculated using 0.231 as the value for θ. * PICO method, Sugaya's adaptation of PICO method, Dumont's method, Parada's centre line method and Barchilon's method.

By providing a conversion framework, our table allows clinicians to convert different measurement methods directly, reducing discrepancies in diagnosis and treatment planning. This is particularly relevant in surgical decision-making, where the extent of glenoid bone loss can influence whether a soft tissue repair or a bony augmentation procedure is preferred.

Despite these advantages, certain limitations must be acknowledged. First, while the conversion table provides mathematical conversions, measurement variability in clinical practice - such as differences in imaging resolution or manual landmark identification - could introduce minor inconsistencies. Due to the exact and mathematical basis of the conversion table, this could potentially be considered an absolute truth and the unavoidable variations in the underlying manual measurements might be neglected. Furthermore, especially the glenoid index method was simplified to offer a reference value in this conversion table. There is, however, mounting evidence that the inferior glenoid circle drawn on the injured glenoid might not accurately represent the original circle of this glenoid before the injury. Future research should focus on validating the existing indexes based on this conversion table in prospective clinical settings, especially assessing this issue.

Conclusion

This study presents a novel conversion table for glenoid bone loss assessment by establishing correlations between commonly used indexes. By bridging the gap between different assessment techniques, this work contributes to a more universal evaluation of glenoid bone loss in shoulder instability management.

Open access statement

This is an open-access article distributed under the terms of the Creative Commons Attribution Licence for Commercial and Non-Commercial Purposes (**CC BY 4.0**, see https://creativecommons.org/licenses/by/4.0/), which allows free use, distribution, adaptation, and commercial use of a work, provided proper credit is given to the creator.

Funding

The authors received no financial support for the research, authorship, and/or publication of this article. This research received no specific grant from any funding agency in the public, commercial, or not-for-profit sectors.

Conflict of Interest

The authors or any member of their families received no financial remuneration related to the subject of the article. The authors or any member of their families have no conflicts of interest to declare.

Ethical Approval

The ethical committee of the UZ Gent approved the study on 08/06/2015. Study number: B670201524915.

References

1. Tennent DJ, Donohue MA, Posner MA. Bone Loss and Glenohumeral Instability. Sports Med Arthrosc Rev. 2017;25(3):131-135. doi:10.1097/JSA.0000000000000156
2. Moya D, Aydin N, Yamamoto N, Simone JP, Robles PP, Tytherleigh-Strong G, et al. Current concepts in anterior glenohumeral instability: Diagnosis and treatment. SICOT J. 2021;7:48. doi:10.1051/sicotj/2021048
3. Di Giacomo G, Piscitelli L, Pugliese M. The role of bone in glenohumeral stability. EFORT Open Rev. 2018;3(12):632-640. doi:10.1302/2058-5241.3.180028
4. Di Giacomo G, Itoi E, Burkhart SS. Evolving concept of bipolar bone loss and the hill-sachs lesion: From “engaging/non-engaging” lesion to “on-track/off-track” lesion. Arthroscopy. 2014;30(1);90-8. doi:10.1016/j.arthro.2013.10.004
5. Di Giacomo G, De Vita A, Costantini A, De Gasperis N, Scarso P. Management of humeral head deficiencies and glenoid track. Curr Rev Musculoskelet Med. 2014;7(1):6-11. doi:10.1007/s12178-013-9194-7
6. Parada SA, Eichinger JK, Dumont GD, Parada CA, Greenhouse AR, Provencher MT, et al. Accuracy and Reliability of a Simple Calculation for Measuring Glenoid Bone Loss on 3-Dimensional Computed Tomography Scans. Arthroscopy. 2018;34(1):84-92. doi:10.1016/j.arthro.2017.07.032
7. McNeil JW, Beaulieu-Jones BR, Bernhardson AS, LeClere LE, Dewing CB, Lynch JR, et al. Classification and Analysis of Attritional Glenoid Bone Loss in Recurrent Anterior Shoulder Instability. Am J Sports Med. 2017;45(4):767-774. doi:10.1177/0363546516677736
8. Sugaya H. Techniques to evaluate glenoid bone loss. Curr Rev Musculoskelet Med. 2014;7(1):1-5. doi:10.1007/s12178-013-9198-3
9. Sommaire C, Penz C, Clavert P, Klouche S, Hardy P, Kempf JF. Recurrence after arthroscopic Bankart repair: Is quantitative radiological analysis of bone loss of any predictive value? Orthop Traumatol Surg Res. 2012 Sep;98(5):514-9. doi: 10.1016/j.otsr.2012.03.015.
10. Lacheta L, Herbst E, Voss A, Braun S, Jungmann P, Millett PJ, et al. Insufficient consensus regarding circle size and bone loss width using the ratio—“best fit circle”—method even with three-dimensional computed tomography. Knee Surg Sports Traumatol Arthrosc. 2019;27(10):3222-3229. doi:10.1007/s00167-019-05391-9
11. Do WS, Kim JH, Lim JR, Yoon TH, Chun YM. Disagreement Between the Accepted Best-Fit Circle Method to Calculate Bone Loss Between Injured and Uninjured Shoulders. Am J Sports Med. 2023;51(4):885-892. doi:10.1177/03635465221149743
12. Moroder P, Damm P, Wierer G, Böhm E, Minkus M, Plachel F, et al. Challenging the Current Concept of Critical Glenoid Bone Loss in Shoulder Instability: Does the Size Measurement Really Tell It All? Am J Sports Med. 2019 Mar;47(3):688-694. doi: 10.1177/0363546518819102.
13. Weil S, Arnander M, Pearse Y, Tennent D. Reporting of glenoid bone loss measurement in clinical studies and the need for standardization : a systematic review. Bone Joint J. 2022 Jan;104-B(1):12-18. doi: 10.1302/0301-620X.104B1.BJJ-2021-0751.R1.
14. Shaha JS, Cook JB, Song DJ, Rowles DJ, Bottoni CR, Shaha SH, et al. Redefining "Critical" Bone Loss in Shoulder Instability: Functional Outcomes Worsen With "Subcritical" Bone Loss. Am J Sports Med. 2015 Jul;43(7):1719-25. doi: 10.1177/0363546515578250.
15. Li RT, Kane G, Drummond M, Golan E, Wilson K, Lesniak BP, et al. On-Track Lesions with a Small Distance to Dislocation Are Associated with Failure After Arthroscopic Anterior Shoulder Stabilization. J Bone Joint Surg Am. 2021 Jun 2;103(11):961-967. doi: 10.2106/JBJS.20.00917.
16. Frank RM, Basques B, Leroux T, Griffin J, Thorsness R, Verma NN, et al. Complications Following Anterior Shoulder Instability Treatment: Bankart Repair Versus Latarjet. Arthroscopy. 2017;33(10). doi: 10.1016/j.arthro.2017.04.027.
17. Hurley ET, Manjunath AK, Matache BA, Jia NW, Virk M, Jazrawi LM, et al. No difference in 90-day complication rate following open versus arthroscopic Latarjet procedure. Knee Surg Sports Traumatol Arthrosc. 2021 Jul;29(7):2333-2337. doi: 10.1007/s00167-020-06301-0.
18. Harmsen K, Huijsmans PE. Management of Glenoid Defects in Anterior Shoulder Instability: A Review of Current Concepts. Open Orthop J. 2017 Aug 31;11:934-945. doi: 10.2174/1874325001711010934.
19. Bauer S, Collin P, Zumstein MA, Neyton L, Blakeney WG. Current concepts in chronic traumatic anterior shoulder instability. EFORT Open Rev. 2023 Jun 8;8(6):468-481. doi: 10.1530/EOR-22-0084.
20. Scanlon JP, Hurley ET, Davey MS, Gaafar M, Pauzenberger L, Moran CJ, et al. 90-Day Complication Rate After the Latarjet Procedure in a High-Volume Center. Am J Sports Med. 2020 Dec;48(14):3467-3471. doi: 10.1177/0363546520964488.
21. Cozzolino A, de Giovanni R, Malfi P, Bernasconi A, Scarpa S, Smeraglia F, et al. Arthroscopic Latarjet Versus Arthroscopic Free Bone Block Procedures for Anterior Shoulder Instability: A Proportional Meta-analysis Comparing Recurrence, Complication, and Reoperation Rates. Am J Sports Med. 2024 Jun;52(7):1865-1876. doi: 10.1177/03635465231188530.
22. Deore VT, Srinivasan S, Pandey R. Latarjet procedure: Current concepts and review. Vol. 5, Journal of Arthroscopy and Joint Surgery. 2018. doi: 10.1016/j.jajs.2018.05.005.

23. Domos P, Lunini E, Walch G. Contraindications and complications of the Latarjet procedure. Shoulder Elbow. 2018 Jan;10(1):15-24. doi: 10.1177/1758573217728716.
24. Alkaduhimi H, Willigenburg NW, Wessel RN, Wolterbeek N, Veen EJD, Koorevaar RCT, et al. Ninety-day complication rate based on 532 Latarjet procedures in Dutch hospitals with different operation volumes. J Shoulder Elbow Surg. 2023 Jun;32(6):1207-1213. doi: 10.1016/j.jse.2022.11.015.
25. Hossein Zadeh R, Daliri M, Sadeghi M, Hossein Zadeh R, Sahebi M, Moradi A, et al. Arthroscopic Bankart repair vs. Latarjet procedure for recurrent shoulder instability: a meta-analysis of clinical outcomes and complication rates in general and athletic populations. J Shoulder Elbow Surg. 2024 Dec;33(12):e652-e674. doi: 10.1016/j.jse.2024.06.024.
26. Arguello AM, Till SE, Reinholz AK, Okoroha KR, Barlow JD, Camp CL. Managing Shoulder Instability in the Overhead Athlete. Curr Rev Musculoskelet Med. 2022 Dec;15(6):552-560. doi: 10.1007/s12178-022-09796-x.
27. Knapik DM, Kuhn AW, Ganapathy A, Gibian JT, Yaeger LH, Matava MJ, et al. Global variations in treatment and outcomes reported for anterior shoulder instability: a systematic review of the literature. JSES Rev Rep Tech. 2023 Sep 16;3(4):469-476. doi: 10.1016/j.xrrt.2023.08.005.
28. Arner JW, Peebles LA, Bradley JP, Provencher MT. Anterior Shoulder Instability Management: Indications, Techniques, and Outcomes. Arthroscopy. 2020 Nov;36(11):2791-2793. doi: 10.1016/j.arthro.2020.09.024.
29. Burkart AC, Debski RE. Anatomy and function of the glenohumeral ligaments in anterior shoulder instability. Clin Orthop Relat Res. 2002;(400):32-9. doi:10.1097/00003086-200207000-00005
30. Bigliani LU, Kelkar R, Flatow EL, Pollock RG, Mow VC. Glenohumeral stability: Biomechanical properties of passive and active stabilizers. Clin Orthop Relat Res. 1996;(330):13-30. doi:10.1097/00003086-199609000-00003
31. Ladd LM, Crews M, Maertz NA. Glenohumeral Joint Instability: A Review of Anatomy, Clinical Presentation, and Imaging. Clin Sports Med. 2021;40(4):585-599. doi:10.1016/j.csm.2021.05.001
32. Makovicka JL, Moore ML, Pollock JR, Rodriguez MJ, Shaha JS, Haglin JM, et al. Magnetic Resonance Imaging Analysis Demonstrates Improved Reliability in Measuring Shoulder Glenoid Bone Loss Using a Two-Thirds Glenoid Height Technique Compared to the "Best-fit Circle." Arthroscopy. 2024;40(3):666-671. doi:10.1016/j.arthro.2023.06.048
33. Green GL, Arnander M, Pearse E, Tennent D. CT estimation of glenoid bone loss in anterior glenohumeral instability. Bone Jt Open. 2022;3(2):114-122. doi:10.1302/2633-1462.32.BJO-2021-0163.R1
34. Chuang TY, Adams CR, Burkhart SS. Use of Preoperative Three-Dimensional Computed Tomography to Quantify Glenoid Bone Loss in Shoulder Instability. Arthroscopy. 2008;24(4):376-82. doi:10.1016/j.arthro.2007.10.008
35. Baudi P, Righi P, Bolognesi D, Rivetta S, Rossi Urtoler E, Guicciardi N, et al. How to identify and calculate glenoid bone deficit. Chir Organi Mov. 2005;90(2):145-52.
36. Shin SJ, Kim RG, Jeon YS, Kwon TH. Critical Value of Anterior Glenoid Bone Loss That Leads to Recurrent Glenohumeral Instability After Arthroscopic Bankart Repair. Am J Sports Med. 2017 Jul;45(9):1975-1981. doi: 10.1177/0363546517697963.
37. Rabinowitz J, Friedman R, Eichinger JK. Management of Glenoid Bone Loss with Anterior Shoulder Instability: Indications and Outcomes. Curr Rev Musculoskelet Med. 2017;10(4):452-462. doi:10.1007/s12178-017-9439-y
38. Itoi E, Lee SB, Berglund LJ, Berge LL, An KN. The effect of a glenoid defect on anteroinferior stability of the shoulder after Bankart repair: a cadaveric study. J Bone Joint Surg Am. 2000 Jan;82(1):35-46. doi: 10.2106/00004623-200001000-00005.
39. Gouveia K, Abidi SK, Shamshoon S, Gohal C, Madden K, Degen RM, et al. Arthroscopic Bankart Repair With Remplissage in Comparison to Bone Block Augmentation for Anterior Shoulder Instability With Bipolar Bone Loss: A Systematic Review. Arthroscopy. 2021 Feb;37(2):706-717. doi: 10.1016/j.arthro.2020.08.033.
40. Levy BJ, Grimm NL, Arciero RA. When to Abandon the Arthroscopic Bankart Repair: A Systematic Review. Sports Health. 2020 Sep/Oct;12(5):425-430. doi: 10.1177/1941738120940676.
41. Gereli A, Yozgatli TK, Yilmaz E, Gamli A, Bayram B, Kocaoglu B. Glenoid bone loss and Hill-Sachs width percentage score are useful to select optimal operation for the treatment of glenohumeral instability in overhead athletes: Arthroscopic Bankart repair with remplissage versus open Latarjet. Knee Surg Sports Traumatol Arthrosc. 2025 Jan;33(1):371-380. doi: 10.1002/ksa.12333.
42. Chuang TY, Adams CR, Burkhart SS. Use of Preoperative Three-Dimensional Computed Tomography to Quantify Glenoid Bone Loss in Shoulder Instability. Arthroscopy. 2008;24(4):376-82. doi:10.1016/j.arthro.2007.10.008.
43. Gerber C, Nyffeler RW. Classification of glenohumeral joint instability. Clin Orthop Relat Res. 2002;(400):65-76. doi:10.1097/00003086-200207000-00009.
44. Griffith JF, Antonio GE, Tong CWC, Ming CK. Anterior shoulder dislocation: Quantification of glenoid bone loss with CT. AJR Am J Roentgenol. 2003;180(5):1423-30. doi:10.2214/ajr.180.5.1801423.
45. De Filippo M, Castagna A, Steinbach LS, Silva M, Concari G, Pedrazzi G, et al. Reproducible noninvasive method for evaluation of glenoid bone loss by multiplanar reconstruction curved computed tomographic imaging using a cadaveric model. Arthroscopy. 2013;29(3):471-7. doi:10.1016/j.arthro.2012.10.017.
46. Dumont GD, Russell RD, Browne MG, Robertson WJ. Area-based determination of bone loss using the glenoid arc angle. Arthroscopy. 2012;28(7):1030-5. doi:10.1016/j.arthro.2012.04.147.
47. Barchilon VS, Kotz E, Barchilon Ben-Av M, Glazer E, Nyska M. A simple method for quantitative evaluation of the missing area of the anterior glenoid in anterior instability of the glenohumeral joint. Skeletal Radiol. 2008;37(8):731-6. doi:10.1007/s00256-008-0506-8.
48. Sugaya H, Moriishi J, Dohi M, Kon Y, Tsuchiya A. Glenoid rim morphology in recurrent anterior glenohumeral instability. J Bone Joint Surg Am. 2003;85(5):878-84. doi:10.2106/00004623-200305000-00016.
49. Bakshi NK, Cibulas GA, Sekiya JK, Bedi A. A Clinical Comparison of Linear- and Surface Area-Based Methods of Measuring Glenoid Bone Loss. Am J Sports Med. 2018 Aug;46(10):2472-2477. doi: 10.1177/0363546518783724.
50. Chalmers PN, Christensen G, O'Neill D, Tashjian RZ. Does Bone Loss Imaging Modality, Measurement Methodology, and Interobserver Reliability Alter Treatment in Glenohumeral Instability? Arthroscopy. 2020 Jan;36(1):12-19. doi: 10.1016/j.arthro.2019.06.025.

51. Verstraeten TRGM, Deschepper E, Jacxsens M, Walravens S, De Coninck B, Pouliart N, et al. Determination of a reference system for the three-dimensional study of the glenohumeral relationship. Skeletal Radiol. 2013;42(8):1061–1071. doi:10.1007/s00256-013-1572-0.

52. De Wilde L, Defoort S, Verstraeten TRGM, Speeckaert W, Debeer P. A 3D-CT scan study of the humeral and glenoid planes in 150 normal shoulders. Surg Radiol Anat. 2012;34(8):743–750. doi:10.1007/s00276-011-0836-4.

53. De Wilde LF, Verstraeten T, Speeckaert W, Karelse A. Reliability of the glenoid plane. J Shoulder Elbow Surg. 2010;19(3):414–422. doi:10.1016/j.jse.2009.10.005.